

Article

# Petrographic Characteristics of Coal Gasification and Combustion by-Products from High Volatile Bituminous Coal

Barbara Bielowicz 

Faculty of Geology, Geophysics and Environment Protection, AGH University of Science and Technology, Al. Mickiewicza 30, 30-059 Kraków, Poland; bbiel@agh.edu.pl

Received: 8 July 2020; Accepted: 23 August 2020; Published: 25 August 2020



**Abstract:** The coal was gasified in a fluidized bed reactor with CO<sub>2</sub> as a gasifying agent at 889–980 °C. The coal and gasification residue produced during gasification was burned at temperatures up to 900 °C. The petrographic analysis, gasification residues, and fly and bottom ash resulting from the combustion of coal and chars showed the efficiency of the gasification and combustion processes. The gasification residue primarily comprised inertoids and crassinetwork, which accounted for 60% of the sample. The analysis of the petrographic composition of fly ash revealed that the fly ash formed during the combustion of gasification residue had a higher mineral content. The fly ash from the combustion of gasification products contained significantly less unburned coal compared to that from coal. The samples of the bottom ash from coal combustion were composed of approximately 25% organic matter, most of which was chars. The bottom ash formed from the combustion of coal gasification products was composed mainly of mineral matter (95% or higher). The obtained results have significant implications in determining future waste management strategies.

**Keywords:** coal; gasification; char; bottom ash; fly ash

## 1. Introduction

Coal gasification, which refers to the transformation of coal into gas, is being increasingly used because of its environmentally friendly nature. The process is conducted using atmospheric air or oxygen as a gasifying agent under specific temperature and pressure conditions. This conversion can be conducted in power plants or directly in the deposit by using energy from the gasified fuel. Using this technology, it is possible to produce synthesis gas that can be used as a fuel or in chemical production.

Coal gasification is affected by many factors other than the parameters of gasification installation itself, including the technological, petrographic, and chemical properties of the raw material subjected to gasification. As the process takes place in stages (degassing, gasification, and combustion of synthesis gas), the coal parameters are influenced by these individual stages. The most important parameters in the gasification process are sinterability, moisture, reactivity, volatile matter content, ash melting point, elemental composition, porosity, and ash and sulfur content [1,2]. The petrographic composition of coal has a significant impact on the gasification process [3]. Coal is a heterogeneous mixture of organic and mineral matter. The organic matter contains vitrinite, liptinite, and inertinite macerals. Generally, coal consists primarily of vitrinite macerals, formed from parenchyma and wood tissues that are composed mainly of cellulose and lignin (e.g., roots, trunks, bark, and leaves). The viability of cell structures depends on the conditions of the decomposition process, the degree of gelification, and the rank of coal. Vitrinite has a high oxygen content compared to other maceral groups. Humification and gelification determine the formation of vitrinite, which, in the process of metamorphism, exhibits characteristic coalification jumps associated with significant oxygen depletion and hydrogen release [4].

The second group of macerals is the liptinite group, which includes macerals of plant origin that contain significant amounts of hydrogen, i.e., cutin, suberin, resins, waxes, fats, and oils. In reflected light, the color of liptinite in low-rank coals is dark gray or gray-brown, while in coking coals, the color becomes brighter. Both the reflectivity and density of the liptinite are lower compared to the vitrinite and inertinite groups [5]. The third group of macerals is the inertinite group, which includes macerals that are common in all coals. It contains components derived from plant matter having undergone a process that results in the production of increased carbon content, e.g., strong coalification or fire. The color in reflected light changes from grayish-white to yellowish-white. This group is unreactive or poorly reactive compared to the other two groups [4].

The rank of coal used as fuel determines oxygen and hydrogen content as well as moisture, which affects the efficiency of the gasifier [6]. The total carbon moisture is important as its excess reduces the calorific value of the gas produced; the reduced calorific value is attributed to energy loss and evaporation of excess water [6]. The most important parameter in the gasification and combustion process is the reactivity of coal, which determines the rate of coal reaction with the gasifying agent and the efficiency of the process [7]. The reactivity of coal is largely influenced by its petrographic composition and rank. Generally, the reactivity of coal decreases as the rank of coal increases [8].

When assessing the suitability of coal for the gasification process, the petrographic composition is of great importance because different macerals have different reactivity. The highest reactivity is observed in vitrinite and liptinite macerals. The inertinite macerals are the least reactive but their gasification starts at higher temperatures, which extends the process time [9]. In the gasification process conducted at a temperature below 1000 °C, it is nearly impossible to use coal that contains significant amounts of inertinite macerals.

Gelified and homogenized components with a tendency to crack and inert macerals (inert, mineral substance) are unfavorable for the gasification process. Hence, the highest possible contents of well-preserved plant tissues and spongy-porous basic mass with completely decomposed tissue are desired [10].

Considering the growing number of gasification installations globally and plans to build such an installation in Poland [11], it is important to determine the directions of management of waste gasification installations that are currently in the design stage. Depending on the amount of organic matter contained in the ash, the waste can be used for cement production, as an aggregate or a backfill in closed mines. However, significant amounts of organic matter increase the risk of self-heating and self-ignition. Therefore, determining the amount and type of these components is of great importance. Petrographic analyses must be conducted on the material from both the pilot and demonstration plants to effectively correct the design process. The problem of residues from gasification and combustion processes in the petrographic aspect has long been recognized by the International Committee for Coal and Organic Petrology (ICCP), which, in the framework of Commission III, has been running working groups on this subject. A petrographic analysis of chars has been conducted by the Characterization of Gasification Products Working Group (International Committee for Coal and Organic Petrology) and a classification for coal char has been developed [12]. A working group within the Commission III (WG Identification and Petrographic Classification of Components in Fly Ashes) identifies the organic components in the ashes [13].

This paper presents the results of petrographic analyses of coal, gasification char, and bottom and fly ash generated during the combustion of coal and char. Para-bituminous coal was obtained from the Janina deposit (Southwest Poland) for this study [14]. The Janina deposit is located in the eastern part of the Upper Silesian Coal Basin. The exploited coal is a Middle Pennsylvanian age coal. The random vitrinite reflectance of the examined coal was 0.51%. As vitrinite reflectance measured in coal samples from the Janina deposit was below 0.6%, this coal is sometimes classified as subbituminous coal [15]. However, based on the ISO classification, this coal should be classified as medium-rank D, high volatile bituminous (according to American Society for Testing and Materials (ASTM) D388) [16] or para-bituminous (according to In-Seam Coal Classification) [17]. The coal was subjected to gasification

in a circulating fluidized bed (CFB) pilot plant using CO<sub>2</sub> as a gasifying agent. The obtained gasification residues differ from those previously described in the literature owing to the course of the Boudouard reaction [18–26].

The petrographic analysis was conducted to determine the effectiveness of gasification residue combustion compared to conventional coal combustion by assessing the organic matter remaining in the ashes. This analysis was also important for assessing the possibility of utilizing the resulting waste by considering its chemical and mineral composition. The composition was found to be directly influenced by the content of individual mineral phases and the process parameters of coal-based fuels used. The dominant factor is the temperature of the processes resulting in the transformation of carbonaceous matter into energy and by-products. The content of individual mineral phases, susceptibility to leaching, and content of combustible substances in waste are influenced by the temperature and atmospheric conditions in the reactor where coal gasification occurs. The method of separation of individual components, e.g., post-reaction gases, affects the degree of purity of the products obtained. An increase in coal gasification temperature allows for solid combustion products with increased content of the glassy phase. The amount of fly ash and post-reaction slag depends on the content of non-combustible mineral substances contained in the coal mass subjected to gasification. Numerous studies have been conducted on the petrographic composition of coal combustion waste (fly ash and bottom ash) [27–35]. However, little research has focused on the composition of ash resulting from the combustion of gasification residue [21,36,37].

## 2. Materials and Methods

Bituminous coal (CoJ; Table 1) from the Janina deposit located in southern Poland was used as the starting material. The coal sample was divided into two parts: The first was gasified and gasification products were burned, and the second was only burned. Test samples were obtained during gasification experiments in a pilot installation at the Institute for Chemical Processing of Coal in Zabrze, Poland. To produce synthesis gas, a CFB reactor with CO<sub>2</sub> as the gasifying agent was used. During the tests, the gasification temperature ranged from 889 °C to 980 °C. The coal flow rate was variable and ranged from 125 kg/h to 140 kg/h.

**Table 1.** Symbols of samples.

Symbol	Sample
CoJ	Coal from Janina Mine
GRJ	Gasification residue from the gasification of coal
FACo	Fly ash from coal
FAGR	Fly ash from gasification residue
BACo	Bottom ash from coal
BAGR	Bottom ash from gasification residue

A detailed description of coal gasification has been previously reported [38]. The gasification residue (GRJ) formed during gasification was burned. Furthermore, a coal sample from the Janina deposit was also burned. The combustion process was conducted in a facility located at the Częstochowa University of Technology. The coal and gasification residues were subjected to combustion using CFB technology. The experimental installation for the combustion of coal and char has been discussed in detail previously [39]. During combustion, two types of ash were generated in the boiler: Bottom ash, which settles at the bottom of the boiler, and fly ash, the particles of which are small and carried by the air current. The combustion of chars occurred at a temperature of approximately 780–875 °C, with a fuel stream ranging from 2 kg/h to 3.2 kg/h and a  $\lambda$  ranging from 1.09 to 1.93. Coal (3–7 kg/h) was burned at atmospheric pressure at a temperature of 750–900 °C. All samples were burned in a fluidized bed. This allowed for the reduction of the combustion temperature to 800–900 °C, the reduction of the

combustion chamber dimensions, and the use of inferior quality fuels (contaminated and with lower calorific value).

Table 2 shows the basic parameters for coal and char. The random reflectance of vitrinite in bituminous coal from the Janina deposit, subjected to gasification, was 0.51%. The vitrinite content (mineral matter free) was approximately 64% by volume and the ash content was 13.8% on a dry basis. According to the ISO 11760 classification, the coal is bituminous D, a moderately high vitrinite and medium ash coal.

**Table 2.** Results of proximate and ultimate analyses of coal and the gasification residue [26].

Parameter	Symbol	Unit	CoJ	GRJ
Moisture	$M^{ad}$	%	5.30	0.20
Ash	$A^{db}$	%	13.80	24.10
Volatile matter	$V^{daf}$	%	38.20	1.95
Gross calorific value	$GCV^{daf}$	MJ/kg	31.50	34.40
Carbon content	$C_t^{daf}$	%	79.93	97.30
Hydrogen content	$H_t^{daf}$	%	5.14	0.92
Nitrogen content	$N^{daf}$	%	1.30	1.60
Total sulfur	$S_t^{db}$	%	1.39	1.09
Ash sintering temperature	$t_s$	°C	1170	-
Ash softening temperature	$t_A$	°C	1270	-
Ash melting temperature	$t_B$	°C	1350	-
Ash fluid temperature	$t_C$	°C	1360	-

Ad—air dried, db—dry basis, daf—dry, ash free basis.

A series of microscopic observations were conducted. Coal from the Janina coal mine and gasification residue and ashes from the combustion process were subjected to qualitative and quantitative analyses. Additionally, to supplement the information, X-ray examinations (XRD) were performed. Based on the obtained results, the exact mineral composition of the samples was determined.

The samples were collected manually in accordance with PN-ISO 18283: 2008. Then, they were dried in an air atmosphere at 40 °C for 24 h. The coal samples and gasification residues were manually ground to a particle size of <1 mm. The bottom and fly ash samples were not ground. The collected samples were used to prepare polished sections according to the ISO 7404-2:2009 2009 standard [40]. Petrographic microscopic examinations were performed under ordinary reflected light and fluorescent (blue) light using a Zeiss Opton Axioplan microscope at the AGH University of Science and Technology, the Faculty of Geology, Geophysics and Environmental Protection. The petrographic composition of coal (including maceral groups) was determined following ICCP recommendations and the following standards: ISO 7404-3: 2009, ISO 7404-5: 2009 [41,42]. The collotelinite reflectance was determined based on measurements at 100 points and a standard deviation of 0.05%. The percentage of individual components in the samples was calculated based on observations of 500–600 equally spaced points on the surface of the polished sections. Each preparation was photographed. With the help of computer software, a special 10 × 10 mesh grid that helped to accurately determine the porosity (expressed as a percentage) of the material was applied to each photograph. Microscopic images were taken using a Zeiss AxioCam5 camera.

The analysis of chars was conducted according to ICCP guidelines [12]. The petrographic classification of fly ash and bottom ash was developed according to the guidelines of Suárez-Ruiz et al. [43].

To determine the mineral composition of samples more accurately, X-ray examinations were conducted. The coal and gasification residue samples as well as the previously discussed products of

their combustion were pulverized. Because of the hardness of the tested material, an agate mortar was used to produce finer samples. Qualitative and quantitative X-ray analyses were conducted using an APD diffractometer (Philips X'pert; with a PW 3020 goniometer). Minerals were identified by referencing ICDD, ICSD, and COD databases.

The analysis was performed in an accredited laboratory in accordance with applicable standards of total moisture [44], ash content [45], volatile matter content [46], sulfur content [47], gross calorific value [48], ash fusibility [49], and carbon and hydrogen content [50].

### 3. Results

#### 3.1. Coal (Co)

Preliminary results of microscopic analysis of coal from the Janina deposit subjected to gasification and the resulting gasification residue have already been presented by Bielowicz [26]. In the present study, the coal was dominated by macerals of the vitrinite group (60.96%) (Table 3). The macerals of inertinite and liptinite groups accounted for 28.97 and 4.85%, respectively. The mineral matter was 5.23%. The mineral matter content was determined at 16.42 wt% (8.66% by vol.) according to the ASTM D2799 and the Parr formula. The values obtained using the formula based on the ash content and sulfur content were different because the macerals were impregnated with mineral matter, e.g., dolomite or clay minerals, which disappeared in the tested coal. The dispersed mineralization was difficult to observe during the petrographic examination.

**Table 3.** Petrographic composition of coal from the Janina deposit and the gasification residue [26].

	Coal		Gasification Residue	
	Maceral	Volume %	Component	Volume %
Vitrinite	Telinite	4.66	Tenuisphere	0.45
	Collotelinite	34.27	Crassisphere	0.90
	Collodetrinite	18.81	Tenuinetwork	15.9
	Corpogelinite	0.39	Crassinetwork	25.11
	Gelinite	2.83	Inertoid	34.72
Liptinite	Sporinite	2.99	Fusinoid/Solid	4.26
	Cutinite	0.71	Mixed porous	12.46
	Resinite	0.64	Mixed dense	3.11
	Liptodetrinite	0.49	Mineroid	3.10
	Alginite	0.00		
Inertinite	Fusinite	11.38		
	Semifusinite	7.17		
	Macrinite	2.14		
	Micrinite	1.17		
	Secretinite	0.57		
	Funginite	0.88		
	Inertodetrinite	5.66		
Vitrinite group	60.96			
Liptinite group	4.83			
Inertinite group	28.97			
Mineral matter	5.23			
Vitrinite (mmf)	64.33			
Liptinite (mmf)	5.10			
Inertinite (mmf)	30.57			

The maceral characteristics of coal from the Janina deposit are presented in Figure 1. The X-ray analysis indicated that the bituminous coal sample had the most variable mineralogical composition among all tested samples. The course of the graph was not clear owing to the dense occurrence of low-intensity peaks (especially from 33 degrees and upward). The clearest peak, indicating the intensity of both quartz and illite (Figure 2), was at approximately 27 degrees. The occurrence of silicon dioxide was evidenced by limited peaks of low intensity over the entire length of the graph. The origin of the mineral was suggested to be related to the sand content of the coal. Microscopic examination showed that the grains were of different sizes and were characterized by low reflectance and high relief.

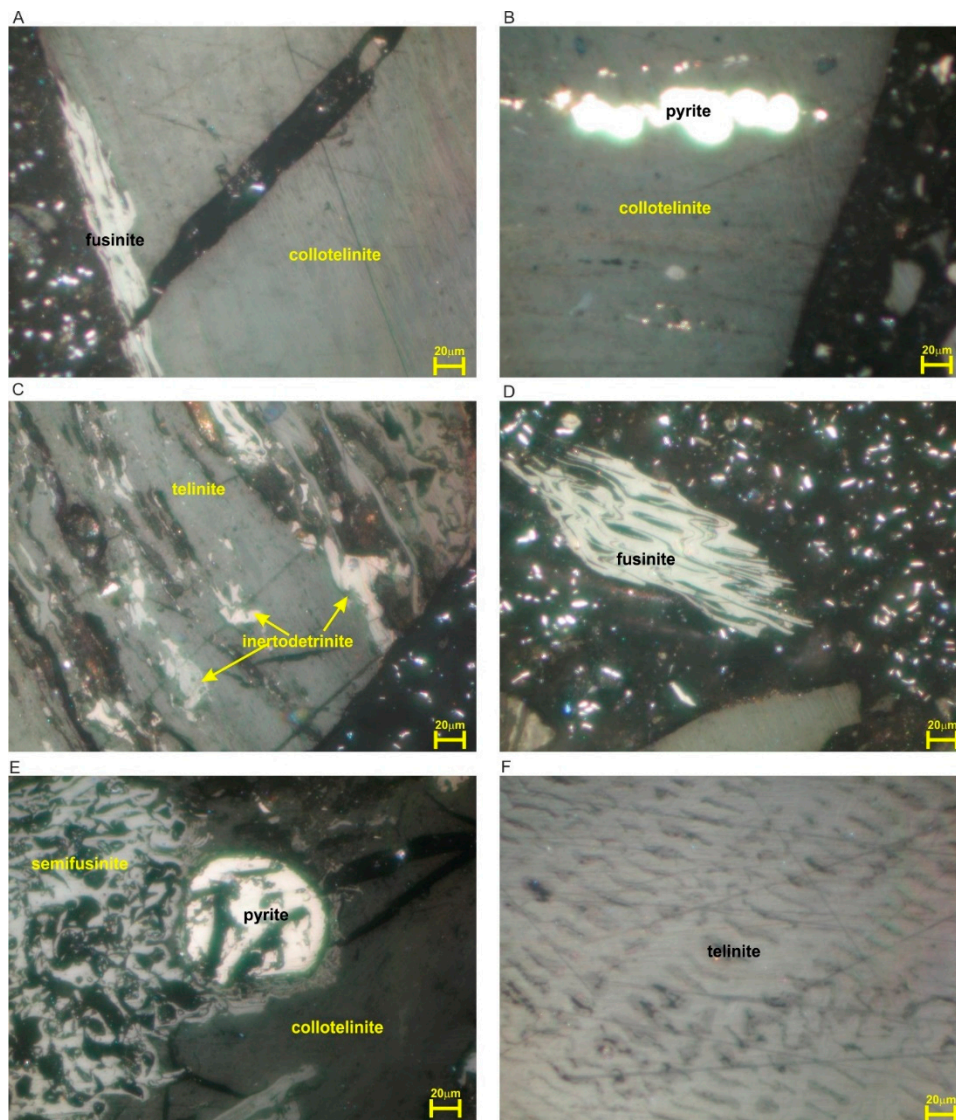


**Figure 1.** Macerals in coal from the Janina deposit: (A) Collotelinite with fusinite (bright), (B) collotelinite with framboidal pyrite (light), (C) telinite (dark) with inertodetrinite (bright), (D) fusinite, (E) semifusinite with pyrite and collotelinite (bright), (F) telinite. Reflected light, oil immersion.

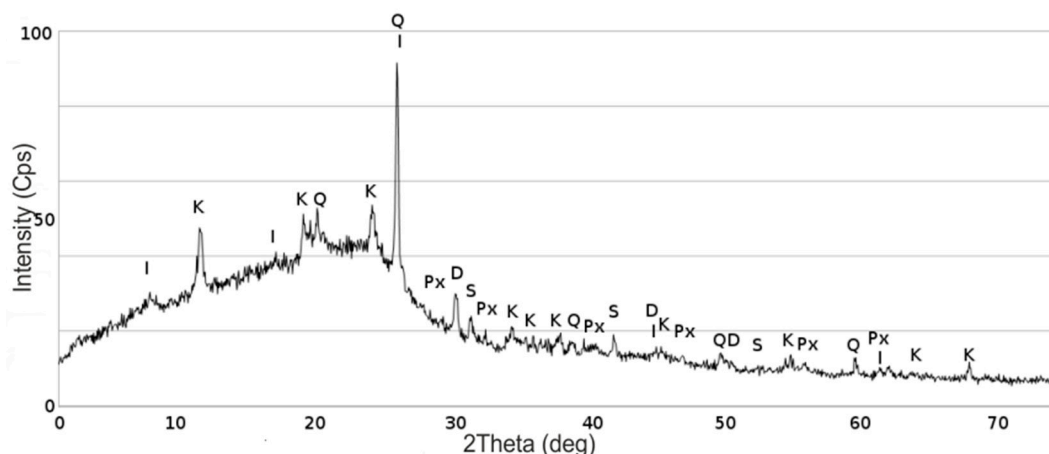


**Figure 2.** X-ray diffraction pattern for bituminous coal sample from the Janina deposit. Q—quartz, K—kaolinite, I—illite, S—siderite, Px—pyrite, D—dolomite.

The high content of clay minerals was especially noteworthy. The occurrence of hydromicas in coal can be a consequence of the inflow of water into peat-bog areas; their increased content has a positive effect on gelification [51]. Kaolinite, the source of the highest number of peaks, was mainly found at lower angles at which several clear signals were observed. Illite occurred in smaller amounts; its presence increased the intensity of the selected diffraction peaks because of the overlap of signals of several crystal forms at the same or similar angles. Illite presence could also be associated with elevated temperatures (150–200 °C) and the occurrence of potassium in colloidal solutions [52]. Microscopic identification of the above-mentioned minerals was complicated because of their fine-grain size and dispersed occurrence. As a consequence, X-ray analysis was used to identify individual clay minerals.

Small peaks indicated the occurrence of pyrite, which appeared in the microscopic images in the form of framboidal pyrite (Figure 1B).

Carbonate minerals, siderite, and dolomite were the least commonly observed. Their occurrence was manifested by a series of almost unnoticeable peaks. Because of their limited occurrence, none of the above-mentioned carbonates were found during microscopic observations. Generally, siderite is the most commonly observed carbonate mineral in coal. Its occurrence suggests the presence of a low-reducing lake and/or marginal lake areas [51]. As an autogenous mineral, it can form both macroscopic and lenticular concretions. The second carbonate determined based on X-ray analysis was dolomite, which is formed via the reaction between magnesium and calcite. Dolomitization could have originated from sedimentation or sediment diagenesis, marine activity, or circulation of magnesium-enriched solutions. The amorphous substance was associated with allophanes, which are amorphous minerals formed from clay minerals (usually kaolinite) [52], amorphous silica, and, to the largest extent, organic matter.

### 3.2. Gasification Residue (GRJ)

Based on the petrographic analysis (Table 3), it can be concluded that the components characterized by low porosity, such as inertoids, were the most commonly observed in the tested material. Approximately 40% of the volume of the gasification residue sample comprised particles characterized by tenuinetwork and crassinetwork arrangements. The sample also contained mixed structures, 15.5% in total. Compared to the starting coal material, a decrease in mineral matter from 5.23% (coal) to 3.1% (mineroid chars) was observed. Moreover, approximately 4% of unburned macerals (solids and macerals that remained unchanged during gasification) were also present in the gasification products. A microscopic image of gasification residue is shown in Figure 3. The ASTM D2799 standard and the Parr formula were used to determine the amount of mineral matter in gasification residues (26.88 wt% mineral matter, (15.06% by vol.)), which was considerably higher than the amount of mineroids. This can be explained by the dispersion, e.g., that of clay minerals, in the chars. Mineral

matter impregnations are most commonly observed in inertoids, which often form aggregates of clay minerals and organic matter.

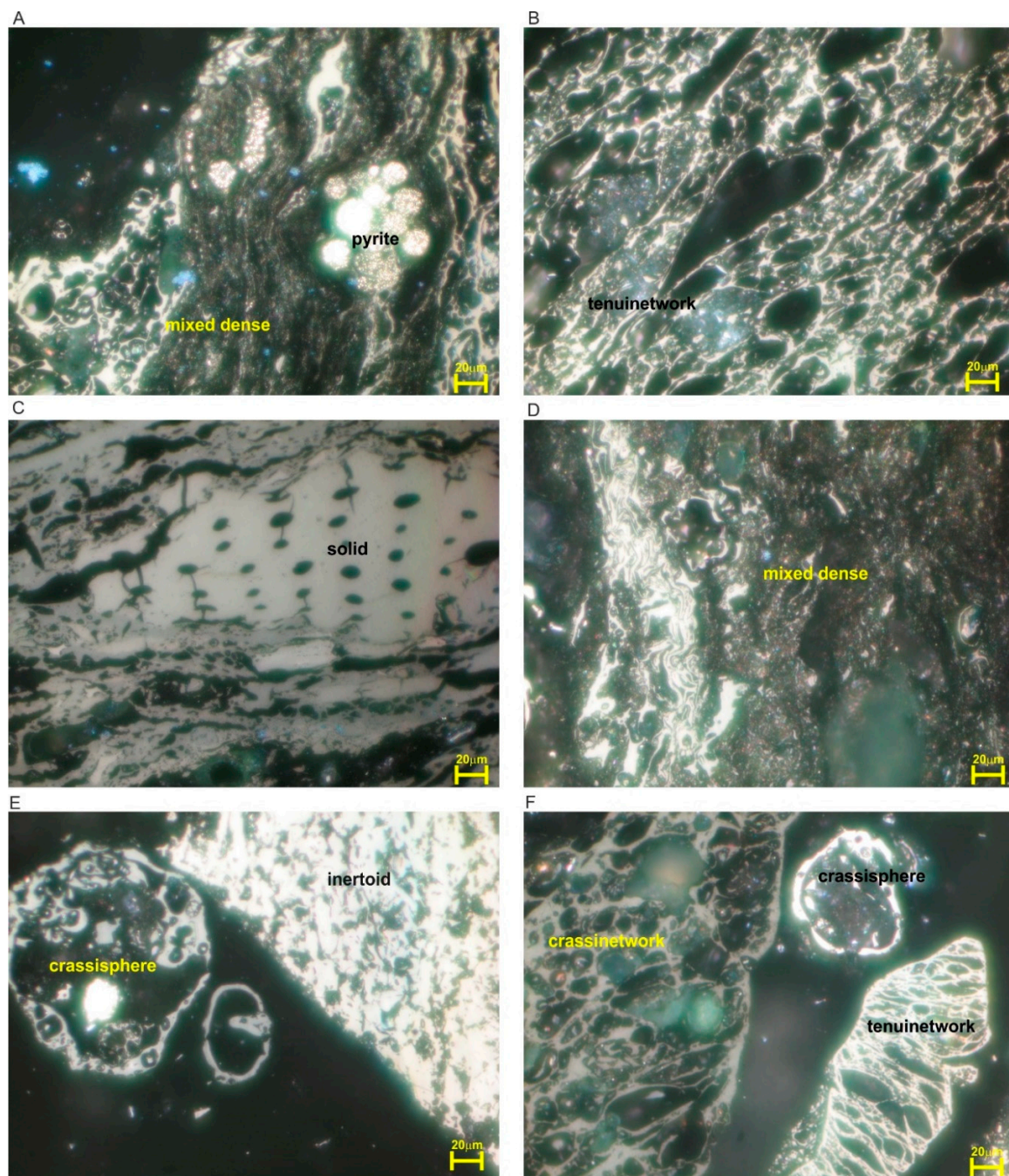


**Figure 3.** Gasification residue components after the gasification of coal from the Janina deposit: (A) Mixed dense with pyrite (bright, spherical), (B) tenuinetwork, (C) solid, (D) mixed dense, (E) inertoid (bright) and crassisphere, (F) crassinetwork (dark), crassisphere (spherical) and tenuinetwork. Reflected light, oil immersion.

The diffraction pattern of the gasification residue sample exhibited a strong impact of amorphous substance (carbonaceous matter) (Figure 4). The graph displayed an irregular pattern and only a few peaks were visible. The mineral composition of the gasification residue was stable. The main mineral was quartz, which was indicated by a clear peak at approximately 27 degrees. The remaining peaks were not very clear. Quartz or inorganic components observed at approximately 27 degrees should be

distinguished carefully when there are no clear graphs to show the crystalline structure of the quartz. Although many mineral phases were altered by the high temperatures during gasification, quartz remained unchanged as it is stable under heat. Microscopic images showed generally rounded quartz grains that were typically in the free space.

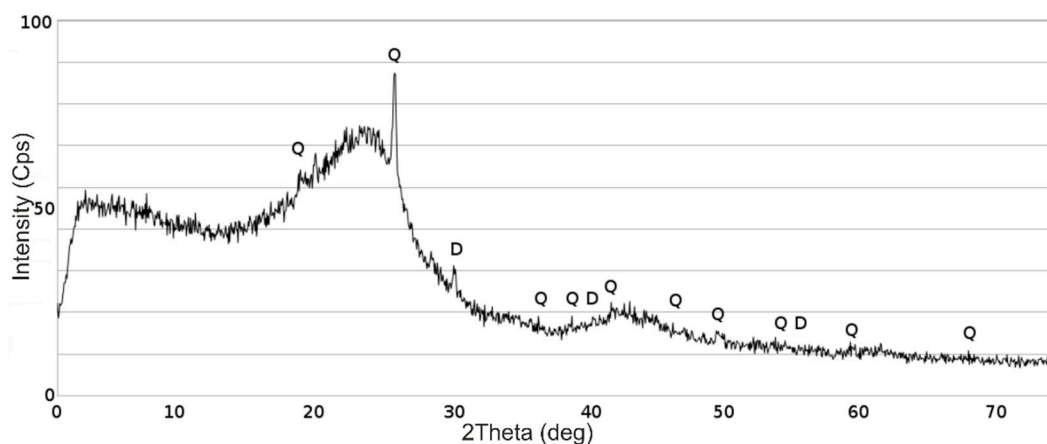


**Figure 4.** X-ray diffraction pattern of gasification residue: Q—quartz, D—dolomite.

Dolomite was also determined using the diffraction pattern. Carbonate was found in small amounts. The intensity of its signals was significantly low, being almost undetectable. A characteristic peak indicated that the mineral was observed only at approximately 31 degrees. Dolomite decomposes at approximately 765–895 °C; therefore, it can be deduced that this temperature was not achieved during the gasification process.

### 3.3. Fly Ash from Coal Combustion (FACo)

Fly ash can be dispersed into the atmosphere along with flue gases. Based on observations, it was found that substances of organic origin constituted a total of 10% of the sample (Table 4).

**Table 4.** Percentages of components in fly and bottom ashes.

	<b>FACo</b>	<b>BACo</b>	<b>FAGR</b>	<b>BAGR</b>
Component	volume %	volume %	volume %	volume %
Mineral matter	90.00	75.80	93.72	95.40
Char	5.98	21.13	5.68	4.46
Unburned coal	4.02	3.07	0.60	0.14

Coal particles are found mainly in tenuinetwork structures. Individual fine structures forming a tenuisphere are less commonly observed. The diameter of the largest identified element, having the features of the above-measured component, was 80 µm. On average, this value was several dozen micrometers. These structures exhibited a well-preserved oval shape.

The ashes also contained components characterized by varied morphology (crassinetwork, inertoids) because their structure remained more stable and did not disintegrate. They reached sizes of the order of hundreds of micrometers (usually about 100 µm, with a maximum of 250 µm). However, the share of these components was small (Figure 5). The chips usually had an irregular shape. In the vast majority of cases, the dimensions of grounded coal were of the order of a few to several micrometers. Occasionally, larger fragments (of the order of several dozen micrometers) could also be found.

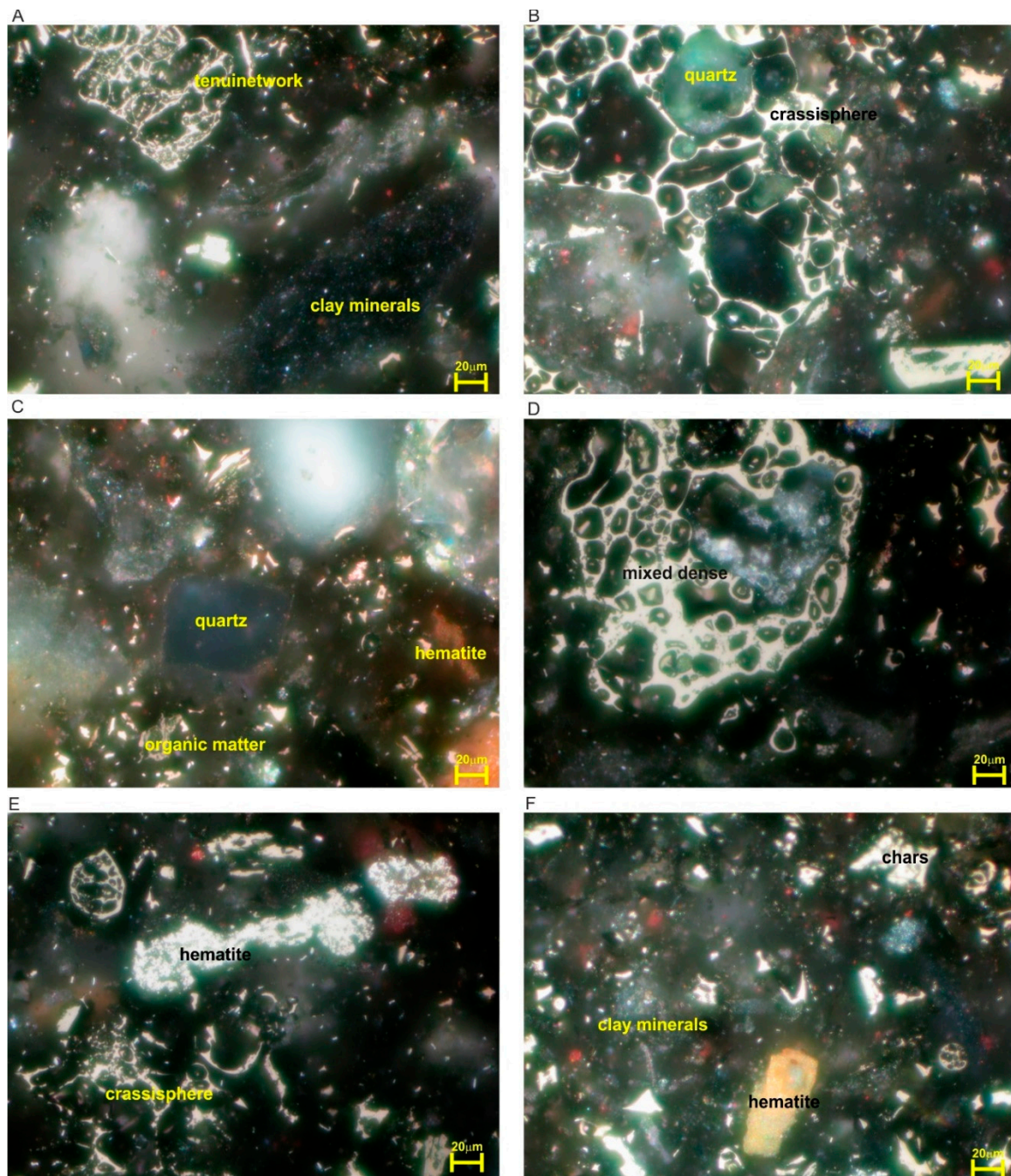


**Figure 5.** Components of fly ash from the combustion of coal from the Janina deposit: (A) Tenuinetwork (bright), clay minerals, (B) crassisphere (bright) with quartz, (C) quartz (central position), a mixture of minerals and organic particles in the background, (D) mixed dense, (E) hematite (bright) and crassisphere, (F) a mixture of clay minerals, iron oxides, and chargs. Reflected light, oil immersion.

The observed minerals formed small, differently shaped grains or aggregates. Quartz and clay minerals were the most commonly observed minerals in the sample (Figure 5). The diffractogram pattern was dominated by clear quartz peaks (Figure 6), while illite and hematite peaks were slightly less intense.

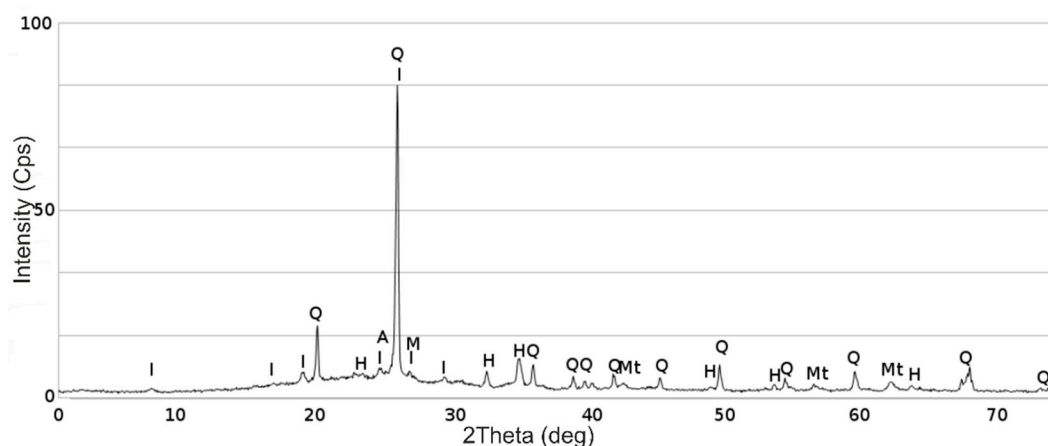


**Figure 6.** X-ray diffraction pattern of fly ash from the combustion of bituminous coal from the Janina deposit. Q—quartz, I—illite, H—hematite, A—anhydrite, M—microcline, and Mt—magnetite.

Peaks from microcline and anhydrite were very small as the signals were weak and almost indistinguishable from background noise. Magnetite was a new mineral identified in contrast with the previous sample and was formed from the decomposition of siderite at a temperature of 450–500 °C. Iron carbonate produces CO<sub>2</sub> and FeO and transforms into magnetite. The newly formed mineral did not change with increasing temperature. It is amorphous and occurs mainly in the form of enamel that takes spherical forms. As in the case of bottom ash, grains were found to be present in the pore space of organic components.

#### 3.4. Bottom Ash Resulting from Coal Combustion (BACo)

Macroscopically, the bottom ash is coarse-grained and brown. Mineral grains on the sanded surface of the preparation usually reach a diameter of about 1 mm, with a maximum diameter of approximately 3 mm. They vary in color, exhibiting yellow through gray to black. Table 4 presents the overall petrographic composition of bottom ash obtained from coal combustion and Table 5 details the share of individual chars.

**Table 5.** Percentage composition of bottom ash resulting from the combustion of coal.

Component	Volume %
Inorganic matter	75.80
Tenuisphere	0.00
Crassisphere	1.07
Tenuinetwork	1.38
Crassinetwork	11.79
Mixed porous	5.82
Mixed dense	0.15
Inertoid	0.92
Fusinoid/Solid	3.07

The inorganic (non-coal) matter comprised most of the ash (approximately 75%). The coal particles mostly exhibited crassinetwork structures. Unburned materials accounted for 3.07% (Table 4).

The term “unburned coal” refers to components that remained unchanged after the combustion process and retained their original form (entire macerals or parts of macerals). Unburned coal components and particles were primarily observed in the form of large chips. Microscopically, these

chips were made of reacted macerals found within a matrix-rich mineral matter. Occasionally, small chips of organic matter could also be found.

The large clusters observed differed in petrographic composition. This was because they originated in different places. Despite the use of the fluidized bed method, the combustion process was incomplete in some areas of the combustion chamber. Generally, mixed porous and crassinetwork structures were the dominant ones (18% of all components) with small amounts of inertoids and crassisphere structures (Table 5).

The main components observed in microscopic images are presented in Figure 7. The structures were characterized by relatively good porosity. Small grains of mineral matter, the size of which was dependent on the size of the pores, were found in the voids. The grains were characterized by relatively uniform roundness and their diameters were in the range of 20–100  $\mu\text{m}$ . The mineral matter was most abundant in pores of crassi-type structures. Crassisphere pores were usually characterized by their irregular shape (Figure 7A); however, forms resembling geometric shapes (rectangles, triangles) could also be observed. Walls building these structures usually reached a thickness of a few to several micrometers. Thicker walls, approximately 20  $\mu\text{m}$  thick, were also observed. Such walls usually contained smaller, oval pores. In the case of “crassinetwork” structures, the parameters were similar, but the structures themselves were larger.

The tenuinetwork was characterized by high porosity (80–90%) (Figure 7D). The structure-building walls were less than 3  $\mu\text{m}$  thick and the pores themselves were smaller compared to those of the crassinetwork discussed earlier. The shapes of structures were very diverse, reminiscent of a spider’s web. The pores were oval or slightly elongated in shape. Mixed structures occurred in small amounts. The material was transformed in varying degrees and the pores had the characteristics of the structures described above.

Particles from the inertoid group were also present in small quantities. These were mainly fusinite or semifusinite residues. Largely, macerals were characterized by unchanged appearance, which made them easy to identify. Fusinite fragments with very well-preserved cellular structures could also be observed. The voids in maceral cells were filled with iron sulfide. Pyrite, under high temperature, transforms into hematite; however, sometimes, it remains in intercellular spaces (Figure 7C). The pyrite in the pore spaces, e.g., semifusinite-like, did not always convert to iron oxides (Figure 7C,F). This was most likely caused by the hindered access of oxygen to the pyrite enclosed in the pores and relatively short combustion time. The vitrinite group was represented by the occurrence of corpogelinite-like clusters (Figure 7B). Its main feature, the oval shape, remained unchanged compared to that of the bituminous coal. Sometimes the material found there was characterized by clearly visible primary structures. It was observed that the components were arranged in parallel along a certain line. This was because of the insufficient transformation of the material. As a result, its arrangement, which corresponded to the thickness of the seam, could be observed. The elongated components were probably formed as a result of the transformation of macerals of the liptinite group (especially cutinite, which was characterized by a linear-parallel arrangement along the seam).

The graph obtained via the X-ray examination was characterized by clear peaks and a smooth background (Figure 8). The main minerals found in the sample were quartz and illite. As in the case discussed earlier, a great elevation (indicating an increase in the intensity of both minerals) could be observed at approximately 27 degrees. Between 10–40 degrees, several small peaks originated from the aforementioned hydromica. Silicon dioxide signals appeared regularly almost throughout the diffraction pattern and could be differentiated from the background noise. Microscopic examination confirmed that quartz grains were the most common mineral.

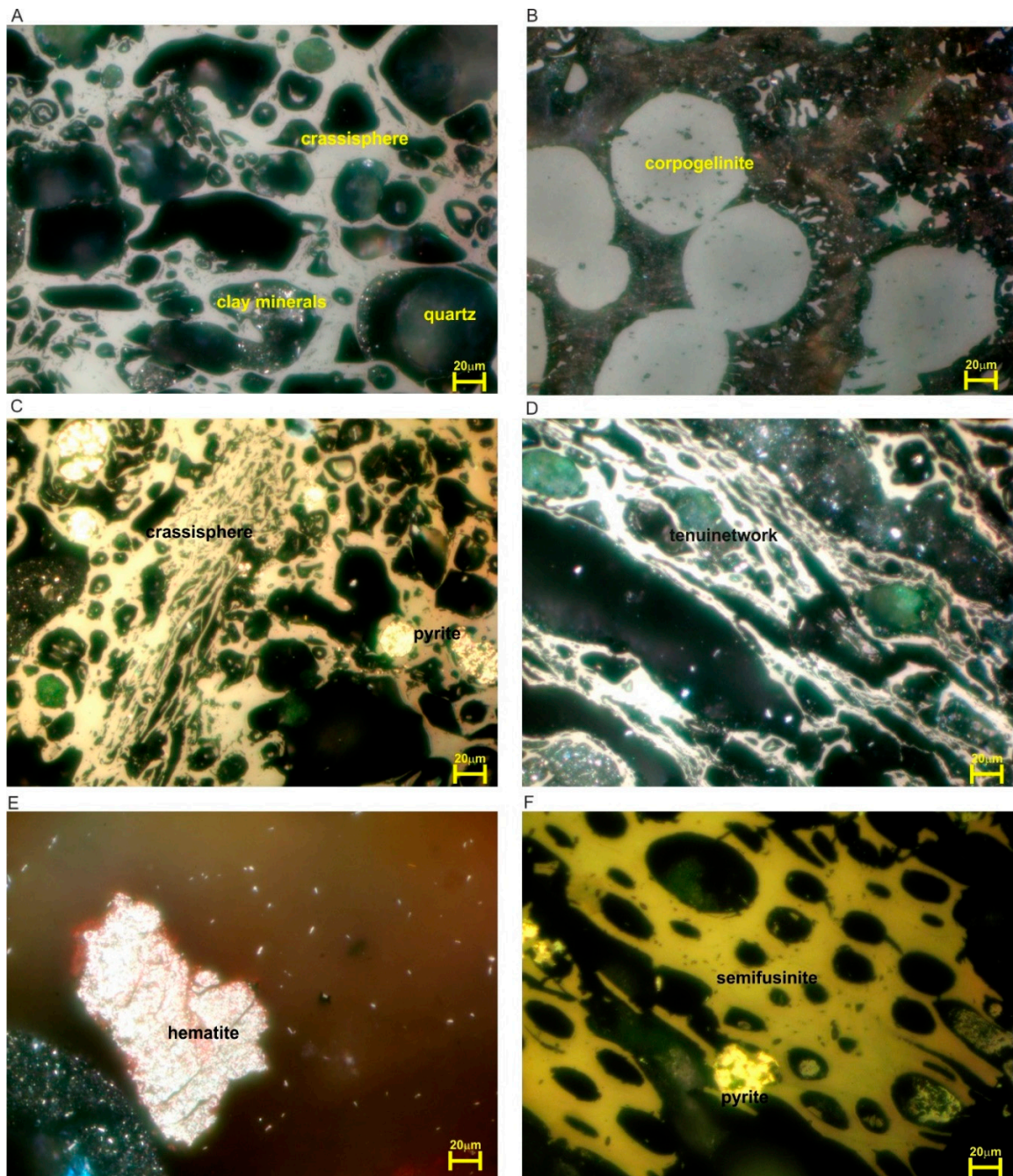


**Figure 7.** Microscopic image of bottom ash from the combustion of coal from the Janina deposit: (A) Quartz and clay minerals in crassisphere pores, (B) corpogelinite-like in a mixture of fine organic particles and argillaceous matter, (C) bright pyrite in crassisphere pores, (D) tenuinetwork, (E) hematite, (F) semifusinite-like with bright pyrite. Reflected light, oil immersion.

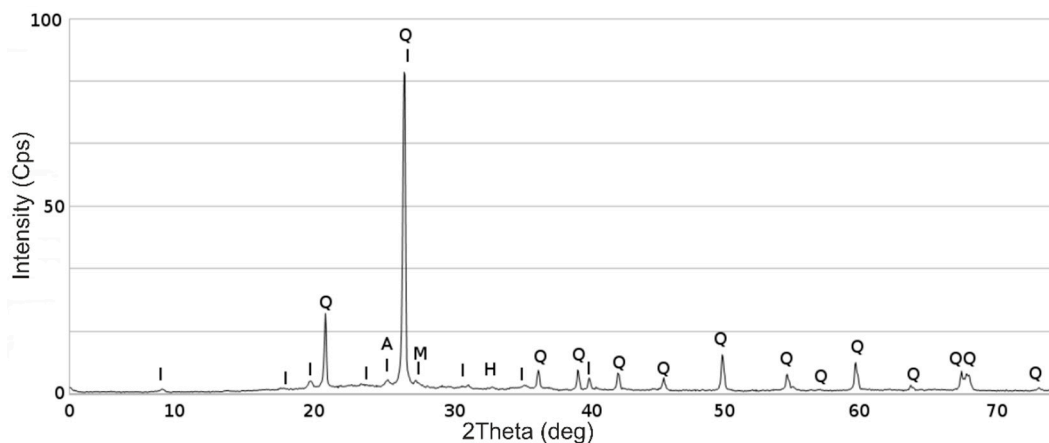


**Figure 8.** X-ray diffraction pattern of bottom ash from the combustion of coal from the Janina deposit, Q—quartz, I—illite, H—hematite, A—anhydrite, and M—microcline.

Hematite was another mineral identified in this study. Iron oxide is formed at a temperature of 500–510 °C as a result of the reaction of pyrite. In this temperature range, sulfide decomposes into hematite and sulfur dioxide with oxygen. Oxide signals were generally weak, slightly distinguishable from the background with only two clear peaks in the graph. Microscopic examination confirmed that hematite formed small clusters located in the pores of chars. It was characterized by high reflectance and a light-yellow and slightly red halo (Figure 7E). Anhydrite and microcline were also determined based on X-ray analysis. The amorphous substance had little influence on the diffraction pattern. It occurred mainly in the form of enamel formed as a result of high temperatures. The grains present were mainly spherical (up to several hundred  $\mu\text{m}$  in diameter), usually occurred individually (often in the pore space of coal particles) and were sometimes hollow.

### 3.5. Fly Ash from the Combustion of Gasification Residue (FAGR)

The fly ash is black and consists of very fine grains that are invisible to the naked eye. The color is associated with the occurrence of unburned carbon grains. The analyzed fly ash from the combustion of gasification ash primarily consisted of mineral matter (Table 4).

Elements of organic origin constituted over 6.28% of the FAGR. The FAGR composition was dominated by gasification residue particles (5.68% on average); the particles ranged in size from a few to several dozen micrometers. In most cases, the FAGR exhibited tenuispheres structures with diameters ranging from a dozen to several dozen (on average approximately 40) micrometers. Locally, larger components with a diameter of 160  $\mu\text{m}$  (Figure 9A) could also be found. Tenuinetwork structures occurred in small quantities. In addition to thin-walled elements, crassispheres could also be observed (Figure 9B). They occurred less frequently but usually were of larger sizes (of the order of 100–200  $\mu\text{m}$ ). In most cases, these structures took the form of rectangles. The thickest walls were approximately 20  $\mu\text{m}$ , with small pores on their surfaces. The burnt coal particles sometimes appeared in the crushed form. Though the continuity of the walls was interrupted, it was possible to identify what type of particle had been ground.

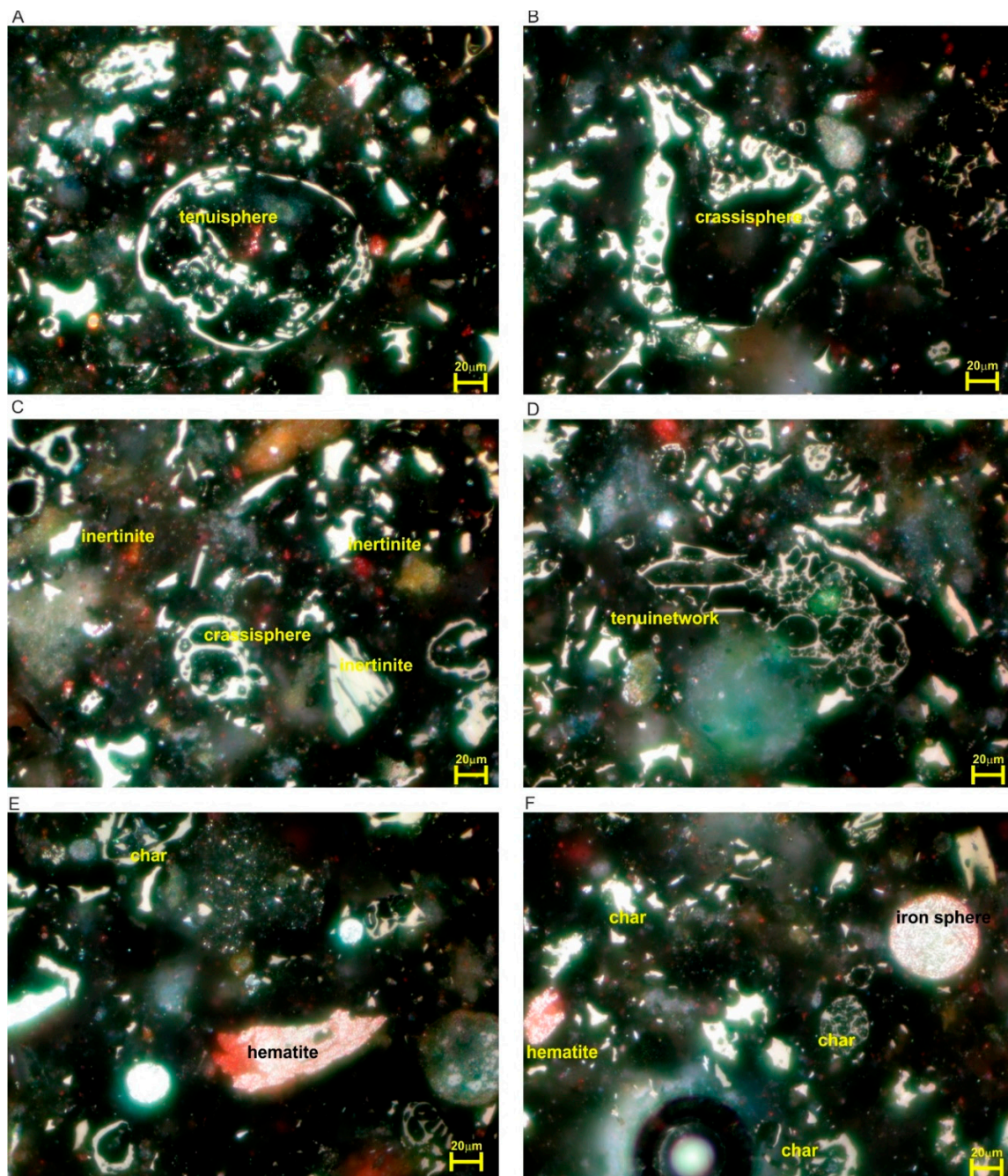


**Figure 9.** Microscopic image of fly ash from the combustion of gasification ash resulting from the gasification of coal from the Janina deposit: (A) Tenuisphere, (B) crassisphere, (C) inertinite chips and crassisphere, (D) tenuinetwork, (E) hematite and a mixture of minerals and chars, (F) hematite (red, left side) organic particles and an iron sphere (spherical, right side). Reflected light, oil immersion.

The proportion of the burnt coal particles was slightly smaller than that of finely ground chars. Their shape was mostly angular (Figure 9C). The examined ash had varying mineralogical composition, and the course of the line of the diffraction pattern also varied (Figure 10). Hematite occurred in the form of small grains characterized by high reflectance. The grains were usually surrounded by a red halo. Locally, spherical hematite could also be found (Figure 9E,F).

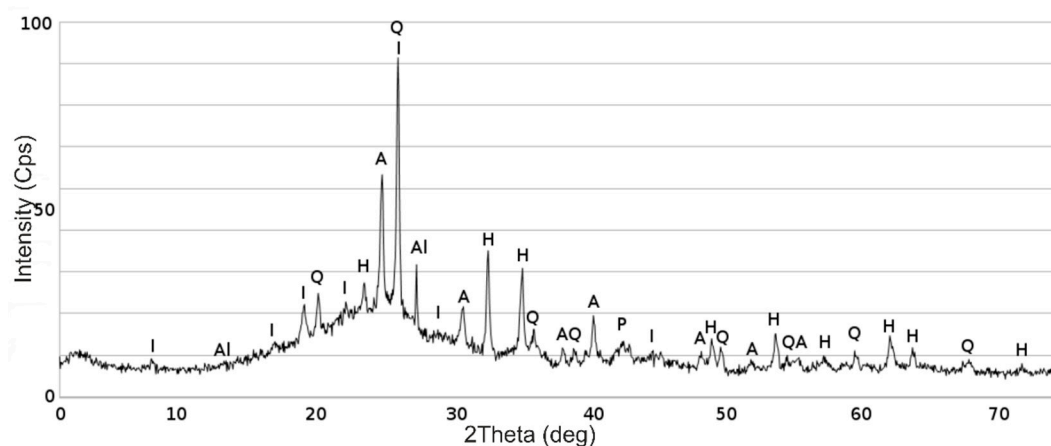


**Figure 10.** X-ray diffraction pattern of fly ash from the combustion of gasification residue resulting from the gasification of coal from the Janina deposit, Q—quartz, I—illite, H—hematite, A—anhydrite, P—periclase, Al—albite.

Quartz in FAGR was less abundant than in the previously analyzed samples. Though its signals were visible, they were not as intense as those recorded for previously investigated research materials.

Illite, represented by several small peaks, could be found in small clusters. Weak signals from anhydrite, at approximately 40 degrees, made it possible to distinguish two distinct peaks from the mineral.

Diffraction studies identified two minerals, periclase and albite, which were not found in coal combustion samples. Peaks from these minerals were densely distributed over almost the entire width of the diffractogram; however, their intensities were very small. As a result, weak signals, that were almost equal to the background noise, were observed. Periclase is a mineral formed by the transformation of dolomite. Bituminous coal and gasification residue samples contained dolomite. This dolomite had not been altered during gasification. It could be assumed that the time spent in the gasification chamber was too short for the transformation of dolomite into periclase. An amorphous substance could create spherical forms or aggregates. Anhydrite was formed during the gasification and the fluidized combustion processes, during which intensive grain movement occurred. Dolomite, or more precisely CaO resulting from its thermal decomposition, enables SO<sub>2</sub> chemisorption. When the fuel grains burned in the fluidized layer, the sulfur compounds contained in them were oxidized and transferred into the gas phase in the form of SO<sub>2</sub>. There were CaO grains around the fuel grains. The resulting sulfur combustion products were immediately adsorbed and chemically bound. As a result, particles of anhydrite were formed, which were removed from the combustion chamber together with ash. Because of the exposure of fly ash from gasification residues to high temperatures for a long time (during gasification and combustion), it was characterized by a higher percentage of altered minerals, such as the periclase, anhydrite, and hematite, compared to fly ash from coal combustion.

### 3.6. Bottom Ash Resulting from the Combustion of Gasification Residue (BAGR)

Bottom ash obtained from the combustion of gasification products had the highest ratio of mineral matter compared to that of other components. Almost 95% of ash components were of inorganic origin (Table 4). Char particles occurred mainly in the form of inertoids (Figure 11A). They formed several relatively large clusters making the analysis of components easier.

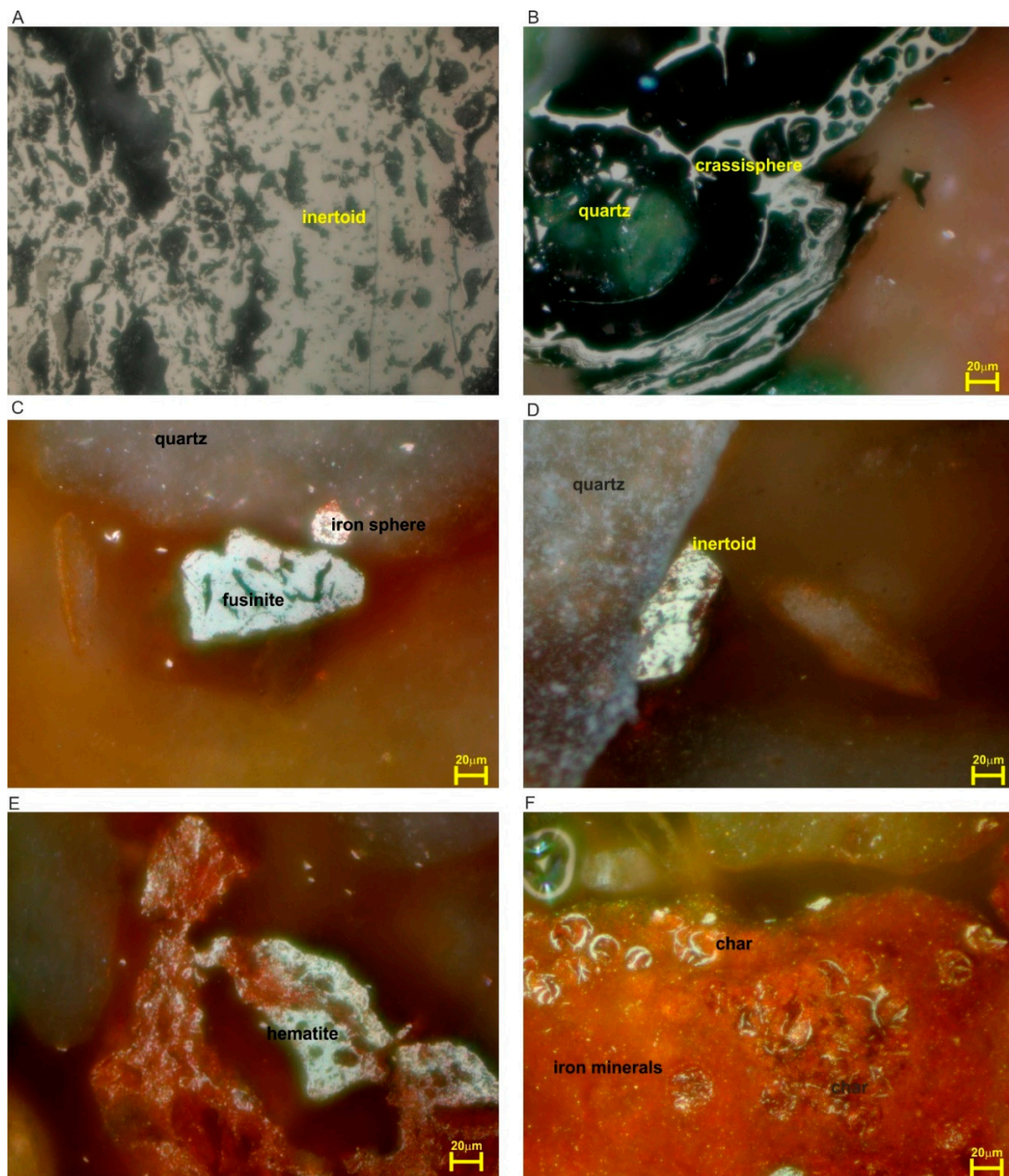


**Figure 11.** Microscopic image of bottom ash from the combustion of gasification residue resulting from the gasification of coal from the Janina deposit: (A) Inertoid, (B) crassisphere, (C) fusinite-like chip with quartz and an iron sphere, (D) inertoid with quartz, (E) hematite, (F) iron minerals with parts of chars. Reflected light, oil immersion.

In addition to the massive inertoids covering relatively large surfaces, chips reaching sizes of the order of several hundred micrometers were also observed (Figure 11D). Ingredients of organic origin were also present, although in very small quantities.

Crassisphere structures occurred in small numbers and constituted a fraction of the overall composition. The walls were usually broken (Figure 11B). Chips of the organic components, mainly those of fusinite-like, were rarely observed. Microscopic observations showed that the preparation had a red-brown color resulting from large amounts of hematite. The main components were quartz, clay

minerals, and iron oxides. The ash diffraction pattern was highly variable (Figure 12) and the most intense signals were from quartz.

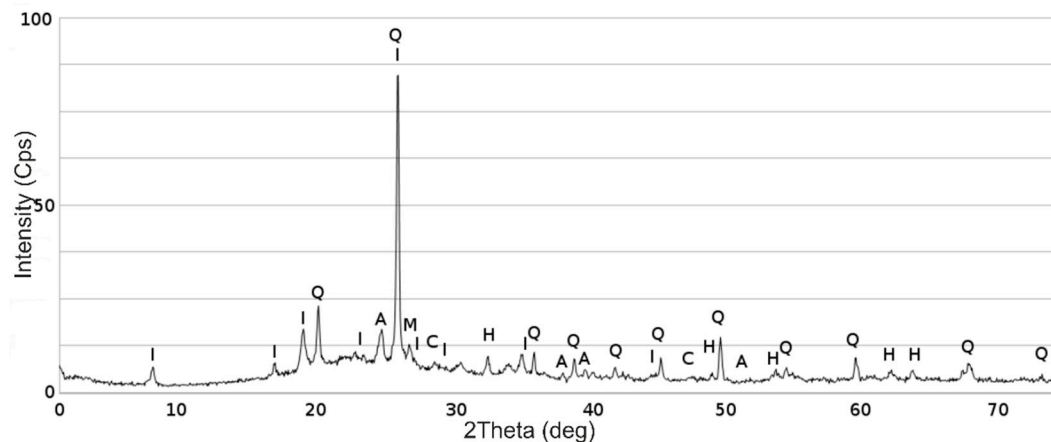


**Figure 12.** X-ray diffraction pattern of bottom ash from the combustion of gasification residue resulting from the gasification of coal from the Janina deposit, Q—quartz, I—illite, H—hematite, M—microcline, A—anhydrite, C—calcite.

Quartz grains have variable shapes and sizes and are generally relatively well-rounded. They filled the majority of the surfaces of the tested preparations. Macroscopically, small (up to 3 mm), white and light-yellow grains could be observed.

The BAGR was also characterized by large amounts of illite. The hydromica signals were quite clear and occurred almost throughout the angular range of the diffractogram. The overlapping intensities of illite and quartz formed the strongest peak at approximately 27 degrees.

Less commonly observed minerals included hematite, microcline, anhydrite, and calcite; the strongest signals were from hematite. Many elements were covered with iron oxide (Figure 11F), as indicated by their red color. The peaks of the other minerals listed above were very weak, only slightly discernable from the background noise. The ash showed the influence of an amorphous substance that was present in the form of aggregates and was associated primarily with the occurrence of enamel formed by high temperature.

#### 4. Discussion

According to Wall [53] and Ladner [54], coal gasification takes place in two successive stages, namely, (1) rapid pyrolysis or degasification of coal and char formation and (2) char gasification. The pyrolysis takes place between 350 °C and 800 °C, and its rate depends on the heating speed, particle size, pressure, and reaction with the gasifying agent. The degree of porosity is an important factor as well [55].

When analyzing the morphology of coal and char components, some regularities were noticed. Individual components obtained during the gasification process (coal particles) retained their characteristic features, which in part allowed the original material to be recognized.

Each group of macerals behaved differently under specific conditions. The components of the former inertinite group were characterized by highest resistance to gasification, whereas the other macerals underwent a more or less visible process of gasification. The most discernible were telinite-like particles, whose cellular structures allowed the accurate penetration of the maceral structure. The porosity and degree of conversion of coal particles in the gasification residue were highly variable. The occurrence of the structures referred to as “tenuinetwork” and “crassinetwork” indicated a favorable petrographic composition of the starting material and desirable conditions for the production of char. Less porous materials (often referred to as “mixed”) are mainly associated with more resistant or less porous macerals (e.g., collotelinite). Macerals of the inertinite group were the

main source of inertoids and solids, i.e., unburned residues. These were the least desirable ingredients found in the char.

The contents of inertoids and solids were highly correlated with the original inertinite content. The reason was the high resistance of these macerals to thermal alteration (gasification or coking). The components were generally characterized by low porosity. Locally, it was possible to determine well-preserved fusinite, whose morphology did not differ from that of the starting material. Fusinite, because of its non-reactive nature in the gasification process, does not show significant changes in the gasification structure. Similar results are also known from the literature. It was also found that other inertinite macerals do not change their original character during the gasification process. This is due to the structure of these macerals, which have a small number of carboxylic and carbonylic groups in their composition. In the cases of chemical processing of coal, such as coking, it has been observed that some inertinite macerals, mainly semifusinite, can be reactive [56,57]. However, it should be noted that the reactivity of coal during gasification is mainly related to the processes occurring on the surface of the particles. The theory of non-reactivity of inertinites in the gasification process is confirmed by the analysis of Raman spectral properties of lignite macerals and the corresponding coal particles in the char produced during the gasification process [23,58].

Some inertoid structures could also be associated with former collotelinite, the large surfaces of which block the effects of gasifying processes. The occurrence of “mixed” and “crassinetwork” structures was largely associated with former macerals of the vitrinite group (the above-mentioned collotelinite). These are structures with high porosity and were observed where the coal had been altered significantly. The crassinetwork could also be associated with former telinite, the cellular structure of which facilitates gas and heat penetration. This maceral was the source of most porous particles (e.g., tenuinetwork), which were the most desirable structures. The alteration of former liptinite macerals is usually accompanied by the formation of porous structures.

The content of gasification residues is related to the chemical composition of the coal subjected to gasification. The coal under investigation can be classified as borderline low-rank/medium-rank coal, in which the aromatic aggregates are mainly single- and two-ring aggregates. At the same time, macromolecules of low-rank coal have irregular shapes, (which is reflected by high porosity and isotropy of this type of coal), a small number of condensed aromatic rings, and numerous heteroatoms [59]. Based on the obtained results, carboxyl groups (COOH) disappear at a temperature of around 350 °C, carbonyl groups (CO) disappear at 500 °C, and the proportion of ether groups (C-OH) increases at 350–500 °C as a result of hydroxyl group condensation. They are stable and are the only groups remaining in coal above 500 °C. Therefore, it is assumed that the ether groups are the main building blocks of the resulting char. Some macerals may have experienced growth in the crystallite size with the increase in temperature, while other coals would have only experienced aromatization [22,60]. This may have a corresponding impact on the variation in reactivity.

In the tested material, there are only a few coal particles that are characteristic of gasification at high temperatures; these have thin walls and very high porosity. Reactions were only observed to take place on the reactive surface of the char. It was also observed that the reactivity of coal increases with increasing temperature [61]. Thus, in the case of gasification in fluidized bed reactors with relatively low temperatures (800–1050 °C), it is necessary to use highly reactive coal with a small amount of inertinite macerals. In the case of coal from the Janina deposit, the share of inertinite macerals is approximately one-third of the sample volume, which means that its gasification at low temperatures and CO<sub>2</sub> atmosphere is not fully effective. A significant amount of macerals from the inertinite group also affects the transformation of mineral matter, especially kaolinite and carbonates. It was noticed that the amount of melted minerals covering the char surface increases with the increase in inertinite content in gasified coal [22].

The bottom ashes resulting from the combustion of coal and gasification residues were characterized by the presence of large mineral grains that were visible to the naked eye. The ashes generated from coal had a higher share (total char and unburned coal: 24.2%) of coal particles than

those resulting from the combustion of gasification residues (total char and unburned coal 4.6%). The bottom ash from the gasification residue had a simpler composition, primarily comprising inertoids. The composition of coal ash was much more diverse, with crassinetwork structures being the most common. The particles themselves occurred in the form of large chips forming fields within the mineral matter. The ashes were composed of quartz, hematite, and illite. Microcline and anhydrite were present in small amounts. Calcite was also found in the ash resulting from the combustion of char.

The shares of chars in FACo and FAGR were similar. The coal ash primarily contained tenuinetwork structures. The FACo was also characterized by a slightly smaller share of unburned coal compared to the reacted particles. In the FAGR, the main coal particles in the ash exhibited tenuisphere structures. The mineral composition of the FACo and the FAGR differed; the common components included quartz, illite, and hematite. Microcline and anhydrite were found in the coal ash, whereas albite and periclase were present in the ash from char. The composition and share of individual components in the tested fly ash differed significantly from those in the ash generated in other installations [32,62–64]. In particular, the examined ashes lacked spherical iron spinels and contained significant amounts of organic matter. The difference in the petrographic composition was a consequence of the relatively low temperature and short combustion time, during which the coal and gasification residues did not fully react. The amount of inertinite macerals also influenced the amount of organic matter in the fly ash. A significant amount of unburned organic matter in the slags resulted from the low-temperature combustion process.

## 5. Conclusions

The sampled coal from the Janina deposit was found to be moderately suitable for the process. The macerals of the inertinite group had a relatively large share of the sample (28.97%), which were easily identified in the gasification products. There was a small share of telinite (4.66%), which, because of its porosity, was found to be a desirable component.

The char composition was dominated by inertoids (about 30%). Crassisphere structures were present in slightly smaller amounts (less than a quarter of samples). Components characterized by high porosity (from the 'tenui' family) constituted approximately 16%.

The analysis has shown that the gasification process involves mainly vitrinite and liptinite macerals, and a higher proportion of aliphatic hydrocarbons were found in their chemical structure. Liptinite macerals, such as resinite, release carboxylic groups during the gasification process, which is indicated by their strong porosity and swelling. A similar phenomenon is observed in the case of telinite. Low porosity macerals, mainly collotelinite, do not significantly increase their porosity and assume the inertoid form in chars. Inertinite macerals do not fundamentally change their structure but increase according to the rank of coal, which is expressed by their higher reflectance in gasification residues compared to the reflectance in the starting coal.

The results indicate that coal from the Janina deposit is not the preferred fuel for the gasification installation using CO<sub>2</sub> as a gasifying agent due to a significant percentage of unreacted macerals in the final product. However, this is only one factor affecting the gasification efficiency. The preparation of the gasified material (grinding and drying) and the conditions of the process also have a considerable influence on its potential for use as a gasification fuel. The reactor in which the process was conducted has serious structural limitations. The geometry of the reactor and the short residence time of the crushed fuel have a significant effect on the gasification process. The temperature of gasification residue combustion was lower than that obtained during coal combustion. Analysis of the ashes indicated that the material obtained from the combustion of gasification residue has a lower content of carbonaceous matter compared to the ashes resulting from the combustion of coal. Currently, coal gasification in the Janina deposit is considered an unprofitable process due to the low calorific value of the obtained chars and the synthesis gas. The problem lies partly in the petrographic composition of coal and the apparatus used to carry out the processes. Because of the use of low-temperature gasification and combustion, the obtained ashes have a low content of glassy components. Depending

on the process conditions, products containing different ratios of the glassy phase to the crystalline phase in the solid waste could be obtained. The phase composition is closely related to the chemical composition of the waste. The properties of the glassy phase are determined by the dominant SiO<sub>2</sub> content. The high content of the glassy phase determines the solubility and, thus, the reactivity of such products, while simultaneously determining the possibility of their use (e.g., inert fillers) for the production of environmentally friendly products, such as building materials and aggregates

Fly ash and bottom ash obtained from the combustion of coal and char also contained organic particles, which indicates the need to modify the combustion process. Coal from the Janina deposit, therefore, had rightly been classified as “conditionally useful.” Despite the relatively large economic (industrial) resources in the deposit (370 Mt), the use of its coal as a fuel for gasification is currently not economically feasible. To use coal from the Janina deposit for gasification in the future, it is necessary to refine the gasification technology itself.

**Funding:** This research was funded by the Polish National Science Centre under the research project awarded by decision no. DEC-2013/09/D/ST10/04045 and from subsidy no 16.16.140.315.

**Acknowledgments:** I would like to thank Grzegorz Tomaszewicz from the IChPW Institute for Chemical Processing of Coal in Zabrze for his help in describing the gasification process.

**Conflicts of Interest:** The author declares no conflict of interest.

## References

1. Higman, C.; van der Burgt, M.; van der Burgt, M. *Gasification*; Gulf Professional Pub./Elsevier Science: Amsterdam, The Netherlands, 2008; ISBN 9780750685283.
2. van Heek, K.H.; Mühlen, H.-J. Aspects of coal properties and constitution important for gasification. *Fuel* **1985**, *64*, 1405–1414. [[CrossRef](#)]
3. Zhuo, Y.; Messenböck, R.; Collot, A.-G.; Megaritis, A.; Paterson, N.; Dugwell, D.R.; Kandiyoti, R. Conversion of coal particles in pyrolysis and gasification: Comparison of conversions in a pilot-scale gasifier and bench-scale test equipment. *Fuel* **2000**, *79*, 793–802. [[CrossRef](#)]
4. Taylor, G.H.; Teichmüller, M.; Davis, A.; Diessel, C.F.K.; Littke, R.; Robert, P. *Organic Petrology: A New Handbook Incorporating Some Revised Parts of Stach’s Textbook of Coal Petrology*; Gebrüder Borntraeger: Berlin, Germany, 1998; ISBN 9783443010362.
5. Stach, E.; Murchison, D.; Teichmüller, M.; Taylor, G.H.; Chandra, D.; Teichmüller, R.; Mackowsky, M.-T.; Teichmüller, M.; Taylor, G.H.; Chandra, D.; et al. *No Title*; Borntraeger: Stuttgart, Germany, 1982.
6. Liu, G.S.; Niksa, S. Coal conversion submodels for design applications at elevated pressures. Part II. Char gasification. *Prog. Energy Combust. Sci.* **2004**, *30*, 679–717. [[CrossRef](#)]
7. Smoliński, A. Coal char reactivity as a fuel selection criterion for coal-based hydrogen-rich gas production in the process of steam gasification. *Energy Convers. Manag.* **2011**, *52*, 37–45. [[CrossRef](#)]
8. Hashimoto, K.; Miura, K.; Xu, J.-J. Gasification reactivity of various coals at a high temperature. *J. Fuel Soc. Jpn.* **1987**, *66*, 418–426. [[CrossRef](#)]
9. Wagner, N.J.; Coertzen, M.; Matjie, R.H.; van Dyk, J.C. Coal Gasification. In *Applied Coal Petrology*; Elsevier: Amsterdam, The Netherlands, 2008; pp. 119–144.
10. Bielowicz, B. Petrographic composition of Polish lignite and its possible use in a fluidized bed gasification process. *Int. J. Coal Geol.* **2013**, *116*, 236–246. [[CrossRef](#)]
11. Ministry of Energy. *Polish Energy Policy until 2040 (Polityka Energetyczna Polski do 2040) PEP2040*; Ministry of Energy: Warsaw, Poland, 2018.
12. Lester, E.; Alvarez, D.; Borrego, A.G.; Valentim, B.; Flores, D.; Clift, D.A.; Rosenberg, P.; Kwiecinska, B.; Barranco, R.; Petersen, H.I.; et al. The procedure used to develop a coal char classification—Commission III Combustion Working Group of the International Committee for Coal and Organic Petrology. *Int. J. Coal Geol.* **2010**, *81*, 333–342. [[CrossRef](#)]
13. Suárez-Ruiz, I.; Valentim, B.; Borrego, A.G.; Bouzinos, A.; Flores, D.; Kalaitzidis, S.; Malinconico, M.L.; Marques, M.; Misz-Kennan, M.; Predeanu, G.; et al. Development of a petrographic classification of fly-ash components from coal combustion and co-combustion. (An ICCP Classification System, Fly-Ash Working Group—Commission III.). *Int. J. Coal Geol.* **2017**, *183*, 188–203. [[CrossRef](#)]

14. Czechowski, F.; Kidawa, H. Reactivity and susceptibility to porosity development of coal maceral chars on steam and carbon dioxide gasification. *Fuel Process. Technol.* **1991**, *29*, 57–73. [[CrossRef](#)]
15. Jelonek, I.; Kruszewska, K.J.; Filipiak, P. Liptinite as an indicator of environmental changes during formation of coal seam No. 207 (Upper Silesia, Poland). *Int. J. Coal Geol.* **2007**, *71*, 471–487. [[CrossRef](#)]
16. ASTM International. *D388-19a Standard Classification of Coals by Rank*; ASTM International: West Conshohocken, PA, USA, 2019. [[CrossRef](#)]
17. UN ECE. *International Classification of in-Seam Coals*; UN ECE: Geneva, Switzerland, 1998.
18. Ściażko, M.; Stępień, L. Boudouard reaction in fluid-bed gasification of coal chars. *Przemysł Chemiczny* **2014**, *93*, 2065–2070. [[CrossRef](#)]
19. Kwiecińska, B.; Petersen, H.I. Graphite, semi-graphite, natural coke, and natural char classification-ICCP system. *Int. J. Coal Geol.* **2004**, *57*, 99–116. [[CrossRef](#)]
20. Everson, R.C.; Neomagus, H.W.J.P.; Kaitano, R.; Falcon, R.; du Cann, V.M. Properties of high ash coal-char particles derived from inertinite-rich coal: II. Gasification kinetics with carbon dioxide. *Fuel* **2008**, *87*, 3403–3408. [[CrossRef](#)]
21. Wagner, N.J.; Matjie, R.H.; Slaghuis, J.H.; van Heerden, J.H.P. Characterization of unburned carbon present in coarse gasification ash. *Fuel* **2008**, *87*, 683–691. [[CrossRef](#)]
22. Oboirien, B.O.; Engelbrecht, A.D.; North, B.C.; Du Cann, V.M.; Verryn, S.; Falcon, R. Study on the structure and gasification characteristics of selected South African bituminous coals in fluidised bed gasification. *Fuel Process. Technol.* **2011**, *92*, 735–742. [[CrossRef](#)]
23. Oboirien, B.O.; Engelbrecht, A.D.; North, B.C.; Du Cann, V.M.; Falcon, R. Textural properties of chars as determined by petrographic analysis: Comparison between air-blown, oxygen-blown and oxygen-enriched gasification. *Fuel* **2012**, *101*, 16–22. [[CrossRef](#)]
24. Malumbazo, N.; Wagner, N.J.J.; Bunt, J.R.R. The petrographic determination of reactivity differences of two South African inertinite-rich lump coals. *J. Anal. Appl. Pyrolysis* **2012**, *93*, 139–146. [[CrossRef](#)]
25. Hower, J.C.; Rathbone, R.F.; Robertson, J.D.D.; Peterson, G.; Trimble, A.S. Petrology, mineralogy, and chemistry of magnetically-separated sized fly ash. *Fuel* **1999**, *78*, 197–203. [[CrossRef](#)]
26. Bielowicz, B. Petrographic composition of coal from the Janina mine and char obtained as a result of gasification in the cfb gasifier. *Gospod. Surowcami Miner.* **2019**, *35*, 99–116. [[CrossRef](#)]
27. Ahn, Y.C.; Lee, J.K. Physical, chemical, and electrical analysis of aerosol particles generated from industrial plants. *J. Aerosol Sci.* **2006**, *37*, 187–202. [[CrossRef](#)]
28. Keppert, M.; Pavlík, Z.; Tydlitát, V.; Volfová, P.; Švarcová, S.; Šyc, M.; Černý, R. Properties of municipal solid waste incineration ashes with respect to their separation temperature. *Waste Manag. Res.* **2012**, *30*, 1041–1048. [[CrossRef](#)] [[PubMed](#)]
29. Ribeiro, J.; Valentim, B.; Ward, C.; Flores, D. Comprehensive characterization of anthracite fly ash from a thermo-electric power plant and its potential environmental impact. *Int. J. Coal Geol.* **2011**, *86*, 204–212. [[CrossRef](#)]
30. Hower, J.C.; Trimble, A.S.; Eble, C.F. Temporal and spatial variations in fly ash quality. *Fuel Process. Technol.* **2001**, *73*, 37–58. [[CrossRef](#)]
31. Mardon, S.M.; Hower, J.C. Impact of coal properties on coal combustion by-product quality: Examples from a Kentucky power plant. *Int. J. Coal Geol.* **2004**, *59*, 153–169. [[CrossRef](#)]
32. Varma, A.K.; Kumar, M.; Saxena, V.K.; Sarkar, A.; Banerjee, S.K. Petrographic controls on combustion behavior of inertinite rich coal and char and fly ash formation. *Fuel* **2014**, *128*, 199–209. [[CrossRef](#)]
33. Cammarota, A.; Chirone, R.; Solimene, R.; Urciuolo, M. Beneficiation of pulverized coal combustion fly ash in fluidised bed reactors. *Exp. Therm. Fluid Sci.* **2008**, *32*, 1324–1333. [[CrossRef](#)]
34. Bilen, M.; Kizgut, S.; Akkaya, B. Prediction of unburned carbon in bottom ash in terms of moisture content and sieve analysis of coal. *Fuel Process. Technol.* **2015**, *138*, 236–242. [[CrossRef](#)]
35. Levandowski, J.; Kalkreuth, W. Chemical and petrographical characterization of feed coal, fly ash and bottom ash from the Figueira Power Plant, Paraná, Brazil. *Int. J. Coal Geol.* **2009**, *77*, 269–281. [[CrossRef](#)]
36. Bunt, J.R.; Wagner, N.J.; Waanders, F.B. Carbon particle type characterization of the carbon behaviour impacting on a commercial-scale Sasol-Lurgi FBDB gasifier. *Fuel* **2009**, *88*, 771–779. [[CrossRef](#)]
37. Wagner, N.J.; Coertzen, M.; Matjie, R.H.; van Dyk, J.C. Chapter 5—Coal Gasification. In *Applied Coal Petrology*; Academic Press: Cambridge, MA, USA, 2008; pp. 119–144, ISBN 9780080450513.

38. Chmielniak, T.; Sobolewski, A.; Tomaszewicz, G. CO<sub>2</sub>-Enhanced coal gasification. Experience of the Institute for Chemical Processing of Coal Zgazowanie węgla przy wykorzystaniu CO<sub>2</sub> jako czynnika zgazowującego. Doświadczenia IChPW. *Przemysł Chem.* **2015**, *1*, 16–22. [CrossRef]
39. Błaszczuk, A.; Nowak, W.; Jagodzick, S. Bed-to-wall heat transfer in a supercritical circulating fluidised bed boiler. *Chem. Process Eng.* **2014**, *35*, 191–204. [CrossRef]
40. ISO. ISO 7404-2:2009—Methods for the Petrographic Analysis of Coals—Part. 2: Methods of Preparing Coal Samples; ISO: Geneva, Switzerland, 2009.
41. ISO. ISO 7404-3:2009—Methods for the Petrographic Analysis of Coals—Part. 3: Method of Determining Maceral Group Composition; ISO: Geneva, Switzerland, 2009.
42. ISO 7404-5:2009—Methods for the Petrographic Analysis of Coals—Part 5: Method of Determining Microscopically the Reflectance of Vitrinite. Available online: <https://www.iso.org/standard/42832.html> (accessed on 30 January 2018).
43. Hower, J.C.; Mastalerz, M. An Approach toward a Combined Scheme for the Petrographic Classification of Fly Ash.). *Energy Fuels.* **2001**, *15*, 1319–1321. [CrossRef]
44. ISO—ISO 579:2013—Coke—Determination of Total Moisture. Available online: <https://www.iso.org/standard/62608.html> (accessed on 17 June 2020).
45. ISO—ISO 1171:2010—Solid Mineral Fuels—Determination of Ash. Available online: <https://www.iso.org/standard/55944.html> (accessed on 17 June 2020).
46. ISO—ISO 562:2010—Hard Coal and Coke—Determination of Volatile Matter. Available online: <https://www.iso.org/standard/55943.html> (accessed on 17 June 2020).
47. ISO—ISO 351:1996—Solid Mineral Fuels—Determination of Total Sulfur—High Temperature Combustion Method. Available online: <https://www.iso.org/standard/4304.html> (accessed on 17 June 2020).
48. ISO—ISO 1928:2009—Solid Mineral Fuels—Determination of Gross Calorific Value by the Bomb Calorimetric Method and Calculation of Net Calorific Value. Available online: <https://www.iso.org/standard/41592.html> (accessed on 17 June 2020).
49. ISO—ISO 540:2008—Hard Coal and Coke—Determination of Ash Fusibility. Available online: <https://www.iso.org/standard/41484.html> (accessed on 17 June 2020).
50. ISO—ISO 609:1996—Solid Mineral Fuels—Determination of Carbon and Hydrogen—High Temperature Combustion Method. Available online: <https://www.iso.org/standard/4724.html> (accessed on 17 June 2020).
51. Wagner, M.; Lipiarski, I.; Misiak, J. *A Petrographic Atlas of Subbituminous and Bituminous Coal from the Polish Deposits and from Uneconomic Occurrences*; AGH: Kraków, Poland, 2008.
52. Jasieńko, S.; Matuszewska, A.; John, A. Properties and structure of hard coals from the borehole Niedobczyce IG-1 in the Rybnik Coal District, Upper Silesian Coal Basin, their petrographic and group constituents. 2. Variations in petrographic composition of the coals along the depth of borehole. *Fuel Process. Technol.* **1995**, *41*, 221–232. [CrossRef]
53. Wall, T.F.; Liu, G.; Wu, H.; Roberts, D.G.; Benfell, K.E.; Gupta, S.; Lucas, J.A.; Harris, D.J. The effects of pressure on coal reactions during pulverised coal combustion and gasification. *Prog. Energy Combust. Sci.* **2002**, *28*, 405–433. [CrossRef]
54. Ladner, W.R.R. The products of coal pyrolysis: Properties, conversion and reactivity. *Fuel Process. Technol.* **1988**, *20*, 207–222. [CrossRef]
55. van Heek, K.H.; Mühlen, H.-J. Effect of coal and char properties on gasification. *Fuel Process. Technol.* **1987**, *15*, 113–133. [CrossRef]
56. Kruszewska, K.J. The reactivity of pseudovitrinite in some coals. *Fuel* **1998**, *77*, 1655–1661. [CrossRef]
57. Kruszewska, K.; Misz, M. Inertynit w procesach koksowania i spalania w świetle badań mikroskopowych. *Zesz. Nauk. Górnictwo Politech. Śląska* **1999**, *243*, 81–89.
58. Bielowicz, B. Changes in the structure of lignite macerals during the gasification process determined by Raman spectroscopy. *Przemysł Chem.* **2019**, *98*, 241–245. [CrossRef]
59. Maciejończyk, N.; Bielowicz, B. Petrographic composition of char from the gasification of coal from the wieczorek mine after combustion. *Gospod. Surowcami Miner.* **2019**, *35*, 69–86. [CrossRef]
60. Sharma, A.; Matsumura, A.; Takanohashi, T. Effect of CO<sub>2</sub> addition on gas composition of synthesis gas from catalytic gasification of low rank coals. *Fuel* **2015**, *152*, 13–18. [CrossRef]
61. Bunt, J.; Waanders, F. An understanding of the behaviour of a number of element phases impacting on a commercial-scale Sasol-Lurgi FBDB Gasifier. *Fuel* **2008**, *87*, 1751–1762. [CrossRef]

62. Misiak, J. Cząstki węglowe w popiołach lotnych ze spalania węgla z polskich złóż. *Gospod. Surowcami Miner.* **2015**, *31*, 111–120. [[CrossRef](#)]
63. Xue, X. Prediction for the burnout of pulverized coal in a coal-fired power plant by combining proximate analysis, coal petrography, and pulverized-coal size distribution. *Energy Sources Part A Recovery Util. Environ. Eff.* **2016**, *38*, 69–74. [[CrossRef](#)]
64. Hower, J.C. Petrographic examination of coal-combustion fly ash. *Int. J. Coal Geol.* **2012**, *92*, 90–97. [[CrossRef](#)]



© 2020 by the author. Licensee MDPI, Basel, Switzerland. This article is an open access article distributed under the terms and conditions of the Creative Commons Attribution (CC BY) license (<http://creativecommons.org/licenses/by/4.0/>).